Study of the Biosorptive Capacity of Avocado Seed (*Persea americana*) for the Removal of Lead (II) from Aqueous Solutions

Tulio C. Paytan Montañez [a,*] Juan Quispe Rodríguez [a] Isaac N. Aliaga Barrera [b] and Golber Rojas Yauri [a]

Ground avocado seeds (*Persea americana*) were evaluated as an adsorbent material for lead (II) ions present in contaminated water. An experimental study was conducted using a 4² factorial design to determine how particle diameters (425 and 125 µm) and the initial metal concentrations (48.8, 195.8, 346.3, and 494.5 mg/L) affect the retention capacities of the biosorbent. Through FTIR spectroscopy, several chemical groups (–OH, –C=O, $–NH_2$, and –COOH) were identified in the biomass. The adsorption capacity was 74.4 mg/g at an initial concentration of 494.5 mg/L, a pH of 4.5, and a particle size diameter of 125 µm, whereas the results obtained with a diameter of 425 µm were lower. The data fitted to the Langmuir model with an R^2 value of 0.9904. This is consistent with an equilibrium description based on homogeneous sites, with a maximum capacity of 73.0 mg/g. Regarding the process rate, the pseudo-second-order kinetic model produced an R^2 value of 0.9474, providing the best fit. It was concluded that avocado seeds constitute a low-cost biosorbent with suitable performance for the removal of lead (II) from contaminated water, representing a sustainable technique for the treatment of heavy-metal containing effluents.

DOI: 10.15376/biores.22.1.169-183

Keywords: Biosorption; Avocado seed; Persea americana; Lead (II), Langmuir isotherm; Pseudo-second-order kinetics; FTIR spectroscopy

Contact information: a: National Autonomous University of Huanta, Huanta, Peru; b: National University of Cañete, Cañete, Peru;
** Corresponding author: tpaytan@unah.edu.pe*

INTRODUCTION

The presence of heavy metals in water bodies has become one of the growing environmental problems in recent years, with significant impacts on both ecosystem and human health. Their occurrence has been reported across different geographical locations. Heavy metals such as lead (II) pose severe toxicity risks in their divalent state and are prone to bioaccumulation in living organisms. Its effects are dose-dependent and have been associated with cardiovascular and renal disorders. Contamination of water sources results from mining and urbanization; therefore, low-cost solutions are being sought to mitigate this problem. The presence of heavy metals in water bodies has become a major environmental concern, particularly when considering conventional water-quality parameters, heavy metal contamination, and sediment pollution (Islam 2026). Water pollution can be further aggravated by turning surface and groundwater sources into resources that require more intensive treatment, alternative sources, or restrictions on use

(Paramanik 2026). Lead (Pb) is a neurotoxic metal that can leach into drinking water from plumbing components, highlighting the need to guide strategies aimed at reducing its presence in low- and middle-income countries (Roy *et al*. 2025). Toxic metals and metalloids can pose a serious threat to human health due to their ubiquitous occurrence (Huang *et al*. 2024).

Water containing heavy metals can be treated through processes such as chemical precipitation and ion exchange, as well as through the use of sophisticated equipment and adsorption techniques involving activated carbon. However, these approaches may represent economic barriers in resource-limited settings, directly affecting communities in developing countries. Approximately 50% of the world's population faces severe water scarcity during at least part of the year, together with widespread water contamination by various toxic chemicals, including heavy metals and metalloids, posing a significant threat to human and environmental health (Li *et al*. 2025). The presence of heavy metals in liquid matrices and their harmful effects on human health remain a major concern (Anbesa *et al*. 2026). Inland freshwater bodies, such as rivers, lakes, and reservoirs, provide a wide range of essential ecosystem services, including drinking-water supply and habitat for aquatic biota, while also supporting various economic activities (Li *et al*. 2026). Organic waste represents a growing challenge, and its reuse has emerged as an imperative need as well as a necessary alternative from both economic and ecological perspectives (Ungureanu *et al*. 2024).

Avocado seed is a by-product generated in tropical regions and is rich in functional groups capable of interacting with metal cations. Numerous plant-derived residues have been investigated for the capture of heavy metals; however, thorough characterization is required to assess their potential as materials for lead (II) removal. Heavy metal contamination remains a major environmental concern. Among these pollutants, lead (Pb^{2+}) is one of the most hazardous toxic metals released into the environment through mining, smelting, fossil fuel combustion, battery manufacturing, and other industrial and urban activities (Vera-Marmanillo *et al*. 2026). The adsorption process for metal removal can be carried out using either batch systems or fixed-bed columns, each of which has different characteristics. Fixed-bed columns are generally more efficient than batch systems for certain contaminants (Cardoso *et al*. 2025). Heavy metals originating from both natural sources, such as mining and volcanic activity, and anthropogenic activities pose serious threats to both human populations and ecosystems (Hira *et al*. 2025).

Conventional water-treatment methods, including ion exchange, chemical precipitation, membrane filtration, and electrochemical treatment, are often highly effective for removing heavy metals from water (Jjagwe *et al*. 2026). Effective solutions require rapid, science-based evidences. However, escalating groundwater dependence and population growth continue to worsen the situation (Sharma *et al*. 2024).

MATERIAL AND METHODS

Biomass Preparation and Conditioning

Avocado seeds were collected in the city of Huanta and subjected to washing and air-drying at an ambient temperature of 22 °C for 6 days, with a moisture content of 4.7 %. Once dried, the seeds were ground using a traditional mill and sieved to obtain particle sizes of 425 μm and 125 μm, to an initial concentration of 494.5 mg/g. The adsorption behavior conforms to the Langmuir isotherm and a pseudo-second-order kinetic model,

suggesting that the process is primarily governed by surface interactions (Dong *et al*. 2026; Molla *et al*. 2026).

Characterization Methods

The various functional groups in the biomass obtained from avocado seeds were characterized using Fourier transform infrared (FTIR) spectroscopy. Other analytical techniques used included proximate and ultimate analyses, Brunauer Emmett Teller (BET) surface area and pore size measurements, scanning electron microscopy (SEM), Energy Dispersive X-ray Spectroscopy (EDS), and batch adsorption experiments.

Biomass preparation was carried out at the physics laboratory of the National Autonomous University of Huanta, while FTIR and SEM analyses were performed in the city of Huancayo Laboratory Slab, National University of Central Peru, using the following equipment: a Shimadzu FTIR spectrophotometer (Model 8400s), a Perkin Elmer spectrophotometer (Model 1600), a Micromeritics BET analyzer (Model GEMINI VII 2390), and a scanning electron microscope (SEM, Model EVO 10Z6).

The mathematical equations for the Langmuir, Freundlich, pseudo-first-order (PFO), and pseudo-second-order (PSO) models are presented. Furthermore, all variables in each equation (such as q_e, C_e, q_{max}, b, K_F, $1/n$, q_t, k_1, and k_2) have been clearly defined: where q_e is the amount of metal adsorbed per unit mass of adsorbent at equilibrium (mg/g), C_e is the equilibrium concentration of the metal in the solution (mg/L), q_{max} is the maximum monolayer adsorption capacity (mg/g), b is the Langmuir constant related to the affinity of the binding sites (L/mg), K_F is the Freundlich constant indicative of the adsorption capacity, and $1/n$ is the heterogeneity factor.

RESULTS AND DISCUSSION

Avocado Seed Particles

Fourier transform infrared spectroscopy

The FTIR spectrum of sample S-4272 exhibited a characteristic carbonyl (C=O) band at 1720 cm^{-1}, indicating a high concentration of ketones and carboxylic acids. A broad and pronounced absorbance band was observed between 3400 and 3240 cm^{-1}, suggesting strong interactions associated with hydroxyl and amino groups. Additional bands were identified at 2920 cm^{-1}, corresponding to C–H stretching vibrations, and at 1620 cm^{-1}, associated with N–H vibrations, confirming the presence of amine or amide groups in this spectral region.

The functional groups –OH, –C=O, $–NH_2$, and –COOH present in the biomass could participate in the binding of metal ions, facilitating adsorption. FTIR spectroscopy has had a significant impact on scientific research and has been applied in a wide range of analytical applications (Giraldo and Marin 2025). Reflectance FTIR has also been used as a rapid technique for classifying grain samples, followed by the development of classification models capable of optimally preserving essential spectral characteristics (He *et al.* 2026). Water-treatment methods, including ion exchange, have been used as accessible approaches for the removal of heavy metals from water (Jjagwe *et al*. 2026). Lead (II) can leach into water from components of different installations, highlighting the need for environmentally friendly strategies to reduce its presence, particularly in low- and middle-income countries (Roy *et al*. 2025).

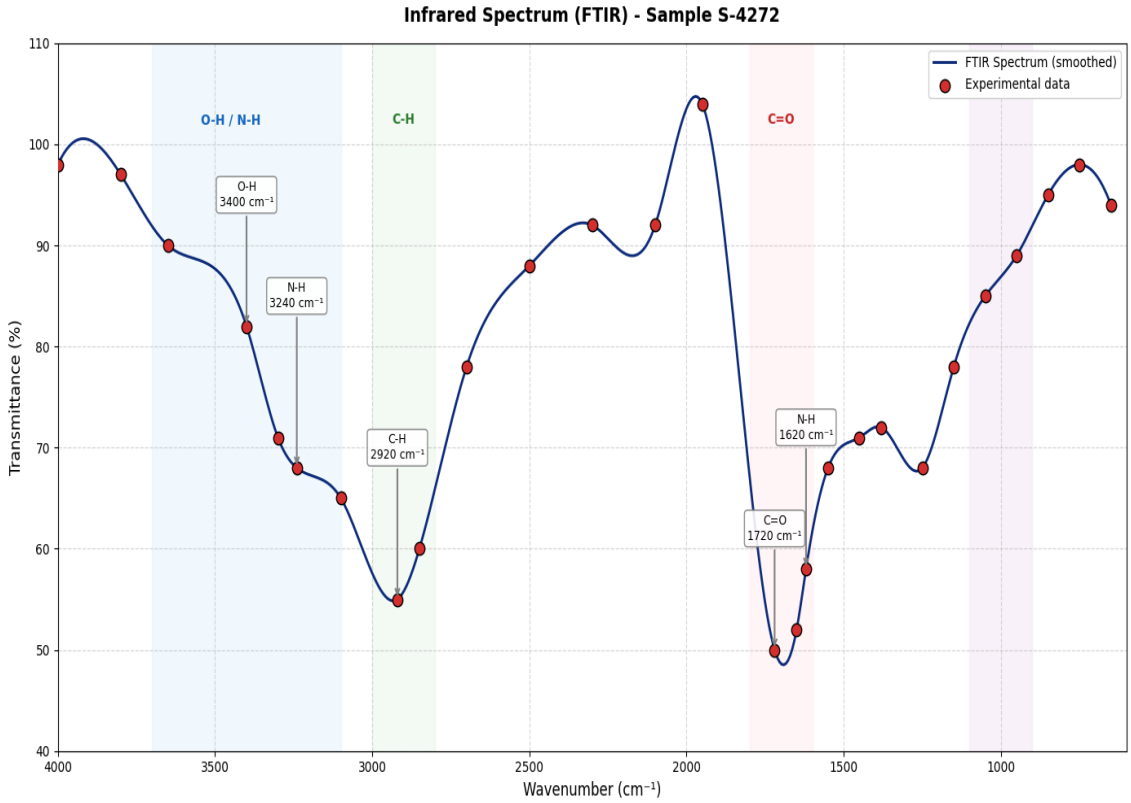


Fig. 1. FTIR infrared spectrum of the avocado seed sample

Figure 1 compares some selected band intensities in an avocado seed specimen. Although an absolute concentration cannot be determined without a calibration curve or absorbance data, the broad and intense band at 3400 cm^{-1} (O–H), together with the contribution at 3240 cm^{-1} (N–H), indicates a high abundance of polar groups (hydroxyl and amine groups). These bands exhibit greater intensity than the aliphatic C–H band at 2920 cm^{-1}, suggesting a structure that is rich in oxygen or nitrogen-containing poses. The intense and sharp band at 1720 cm^{-1} (C=O) reveals an appreciable amount of carbonyl groups (esters, acids, or ketones), while the band at 1620 cm^{-1} (N–H bending or C=C) confirms the presence of amides or unsaturated groups.

Influence of Particle Size

The effect of four particle sizes (PS) of the biomass 425, 300, 250, and 125 µm, were examined. The adsorption process used for different PS sizes followed the Langmuir isotherm model and is a spontaneous and exothermic reaction (Wang *et al*. 2025). Lead (II) retention was evaluated using a solution volume of 0.1 L, an agitation time of 3 h, a stirring speed of 400 rpm, a dose of 0.2 g, and a pH of 4.5. The results revealed an inverse relationship between particle diameter and adsorption capacity. The highest value, 74.4 mg/g, was achieved with the finest particle size of 125 µm and the highest initial concentration of 494.5 mg/L, whereas the 425 µm particles yielded the lowest values. Considering particle size distribution increases the accuracy and prediction speed of the integrated model for adsorbent adsorption behavior, allowing the model to demonstrate strong application potential in the simulation and prediction of fixed-bed adsorption (Zhang and Shu 2025).

Adsorption capacity varied according to particle size. Experimentally obtained adsorption parameters can be used in water-quality models that consider the effects of adsorption processes in sediments. Sediment particles with $D < 500$ μm had adsorption capacities that ranged from 0.15 to 0.47 $mg \cdot g^{-1}$, showing a negative exponential relationship. Kinetic adsorption data for most sediment fractions ($D < 250$ μm) were closely distributed and exhibited a consistent linear trend, allowing unified kinetic adsorption parameters to be determined for non-uniform sediments under different S values: $k1 = 0.257$ $L \cdot mg^{-1} \cdot h^{-1}$ and $k2 = 0.057$ h^{-1} (Xia *et al*. 2026). Ammonia adsorption and its subsequent conversion to NH_4^+ were also observed (Reus *et al*. 2026).

Influence of the Initial Lead (II) Concentration

As the temperature increased at the inflection point, the capacity reached its maximum; the heat of adsorption fluctuated but never dropped to zero, indicating that the heat release induced by physisorption continued to trigger oxidative reactions (Zhang *et al*. 2026).

To begin, lead ion concentrations of 48.8, 195.8, 346.3, and 494.5 mg/L were evaluated using a seed particle size of 125 μm, a pH of 4.5, a dose of 0.18 g, a contact time of 3 h, and an agitation speed of 400 rpm. It was found that the amount adsorbed at equilibrium (q_e) increased with the initial metal concentration, reaching a maximum value of 74.4 mg/g at the highest concentration tested. This trend is attributed to the increased driving force resulting from the concentration gradient, which facilitates the transport of ions toward the adsorbent surface. The upward trend of the curve suggests that, within the studied range, complete saturation of the biomass had not yet been reached. These opposing trends mechanistically highlight the trade-off between surface functionality and porosity (Abu-Shareha *et al*. 2026).

Lead (II) removal reached 54% and subsequently decreased as the monovalent-to-divalent element ratio increased, indicating that dissolved monovalent and divalent cations altered the effective ionic strength of the solution and, consequently, suppressed lead (II) removal. The effect on the maximum adsorption capacity ($mg \cdot g^{-1}$) depended on the biomass content (An *et al*. 2026).

Scanning Electron Microscopic Analysis

The findings from SEM revealed a heterogeneous matrix with a relatively uniform particle distribution and two clearly differentiated phases. The presence of a bright central core indicated a higher atomic number or greater density, while a gray surrounding region with sizes reaching approximately 40 μm was also observed. In the context of avocado seed adsorption, the surface exhibited a heterogeneous morphology. The bright phase indicated the presence of organic compounds, whereas the gray phase corresponded to a carbonaceous organic matrix. The absence of agglomeration suggests an accessible surface, which favors the adsorption of contaminants or ions by increasing interparticle porosity and the availability of adsorption sites, confirming the potential of avocado seed biomass as an adsorbent.

In Fig. 2, the use of backscattered electron (BSE) mode means that the image highlights contrasts based on atomic number. Thus, the results suggest that the observed pores were bounded by phases with different chemical compositions. However, no numerical values were provided for pore size, surface area, percentage porosity, size distribution, or density.

Heavy-metal-contaminated water can be treated using adsorption techniques; however, these methods may impose economic barriers in resource-limited settings, directly affecting communities in developing countries (Li *et al*. 2025). The reuse of waste materials has emerged as a necessary alternative from both economic and ecological perspectives (Ungureanu *et al*. 2024).

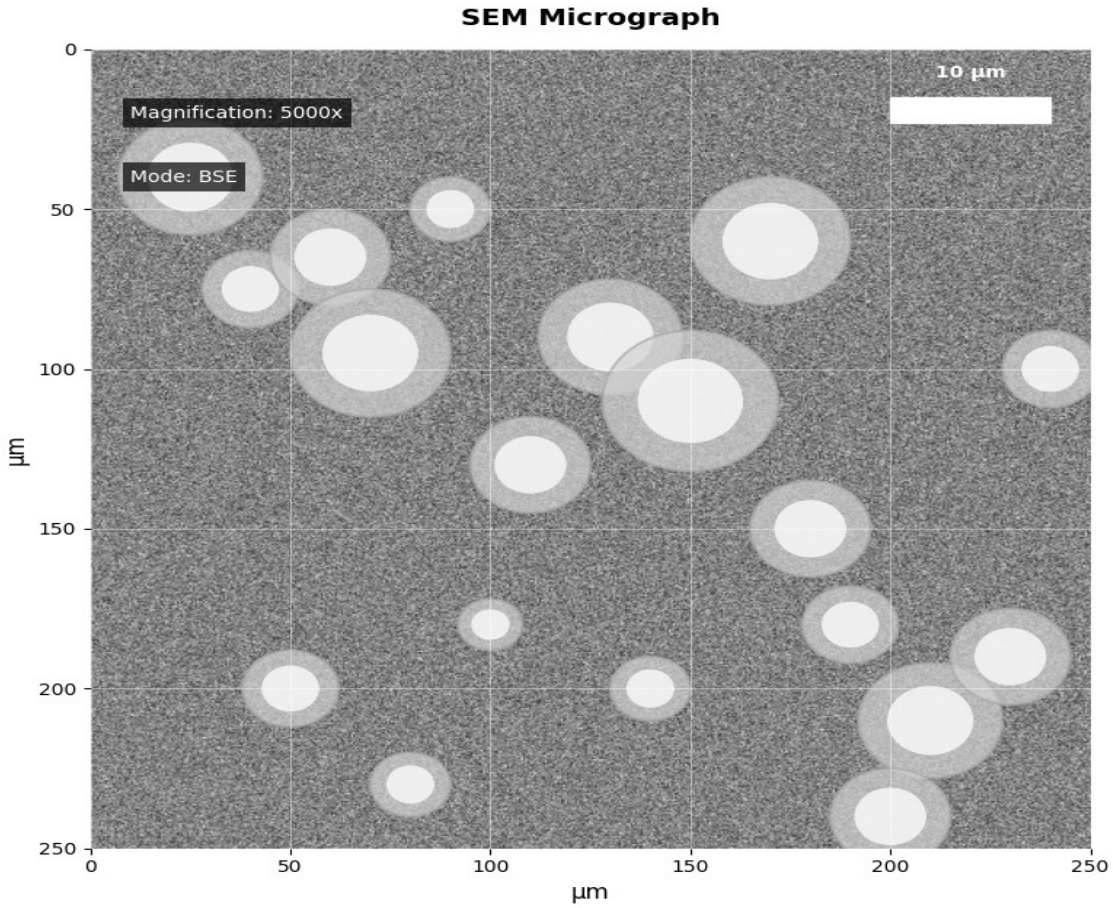


Fig. 2. SEM micrograph of the avocado seed particle

Energy Dispersive X-ray Spectroscopic Analysis

The EDS spectrum quantified the surface composition of the avocado biomass, confirming the nature of the material and its contribution to the porous structure and surface area involved in physical adsorption. The mineral-associated elements present in the biomass may act as active adsorption sites through ion-exchange mechanisms. The results indicate that the biomass surface contains a high density of heterogeneous active sites, which enhances its adsorption capacity and favors metal retention and ion-exchange processes.

The quantitative data show maximum intensity peaks at 4.0 keV (100 cps) and 8.5 keV (60 cps), indicating that the predominant element in the sample is the one generating the signal at 4.0 keV, followed by the element corresponding to 8.5 keV. In contrast, intensities below 30 cps at energies such as 1.5, 2.0, 3.0, and 5.5 keV suggest the presence of minor or trace elements, these values only allow a relative comparison of abundance rather than the determination of absolute concentrations.

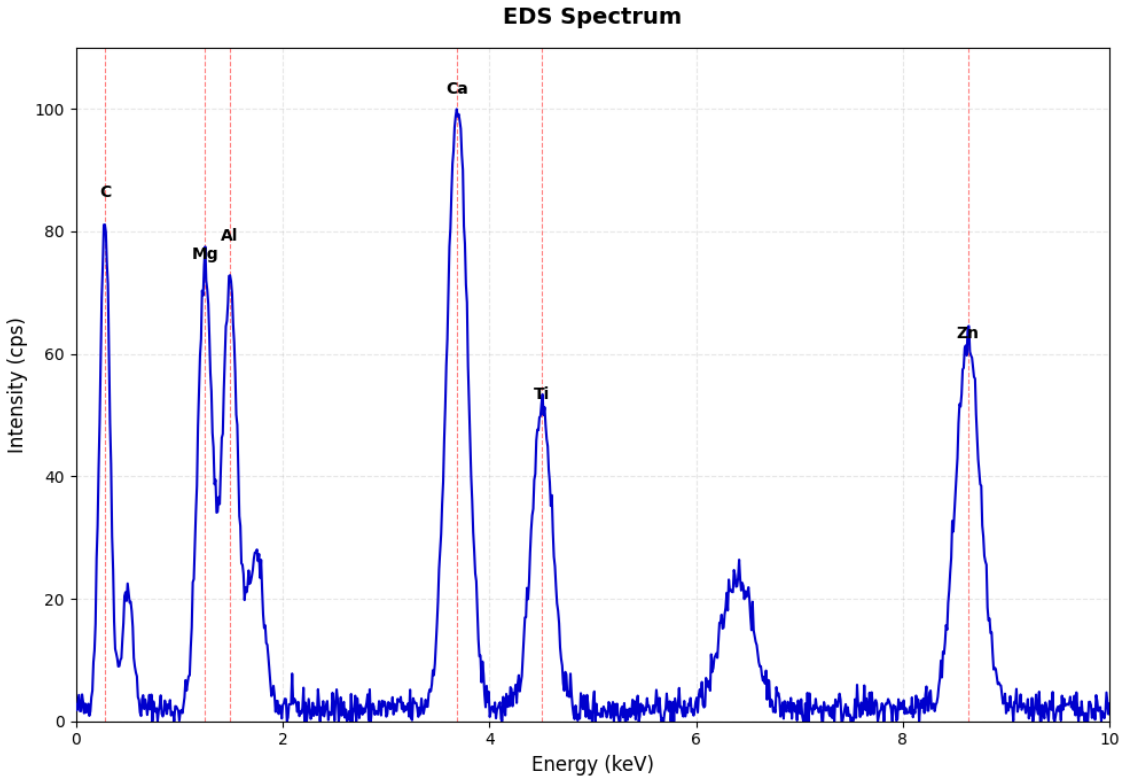


Fig. 3. EDS spectrum of the avocado seed sample

Avocado seed is a by-product generated in tropical regions and is rich in functional groups capable of interacting with metal cations, while heavy metal contamination remains a major environmental concern. Among these contaminants, lead (II) is of particular importance (Vera-Marmanillo *et al*. 2026). Adsorption processes are used for metal removal on surfaces with different physicochemical characteristics (Cardoso *et al*. 2025). Heavy metals pose serious threats to both human populations and ecosystems (Hira *et al*. 2025).

Particle Size Distribution Analysis

The plot of adsorption as a function of mean particle size showed a negative linear relationship (R^2 = 0.983, slope = -1.33). As the particle size increased from 4.5 µm to 15 µm, the adsorption capacity decreased significantly from 50 to 35 mg/g indicating that intraparticle diffusion was a rate-limiting step.

The particle size distribution analysis revealed a mean diameter of 4.2 µm and a median of 3.6 µm, following a log-normal distribution. This indicates that most particles exhibited a relatively homogeneous size distribution. Since the median was lower than the mean, the distribution showed positive skewness, with a predominance of fine particles ranging from 2 to 5 µm. This particle size range was favorable for adsorption because, as particle size decreases, the surface area per unit mass increases, providing a greater number of active sites available for contaminant adsorption. Particles ranging from 15 to 20 µm, with an internal porous structure, also contributed to adsorption capacity through intraparticle diffusion. Therefore, ground avocado seed biomass with an accessible surface area exhibited greater adsorption efficiency, as particle size maximized contact between the adsorbent and the adsorbate in the aqueous solution.

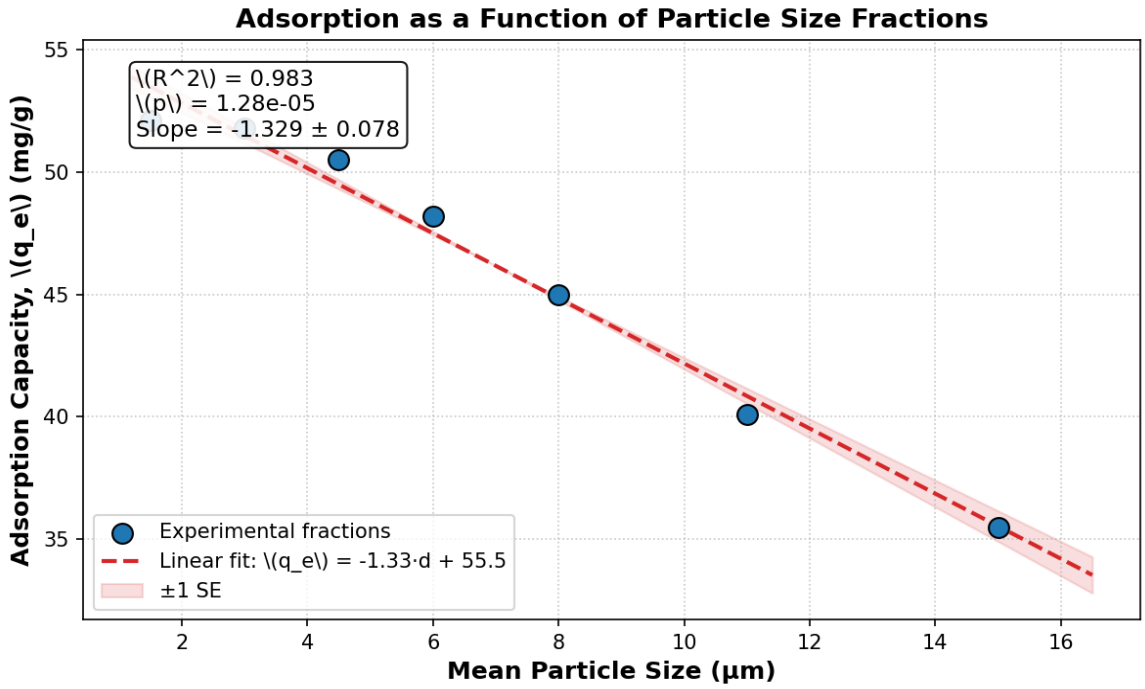


Fig. 4. Adsorption as a function of particle size fractions and adsorption capacity

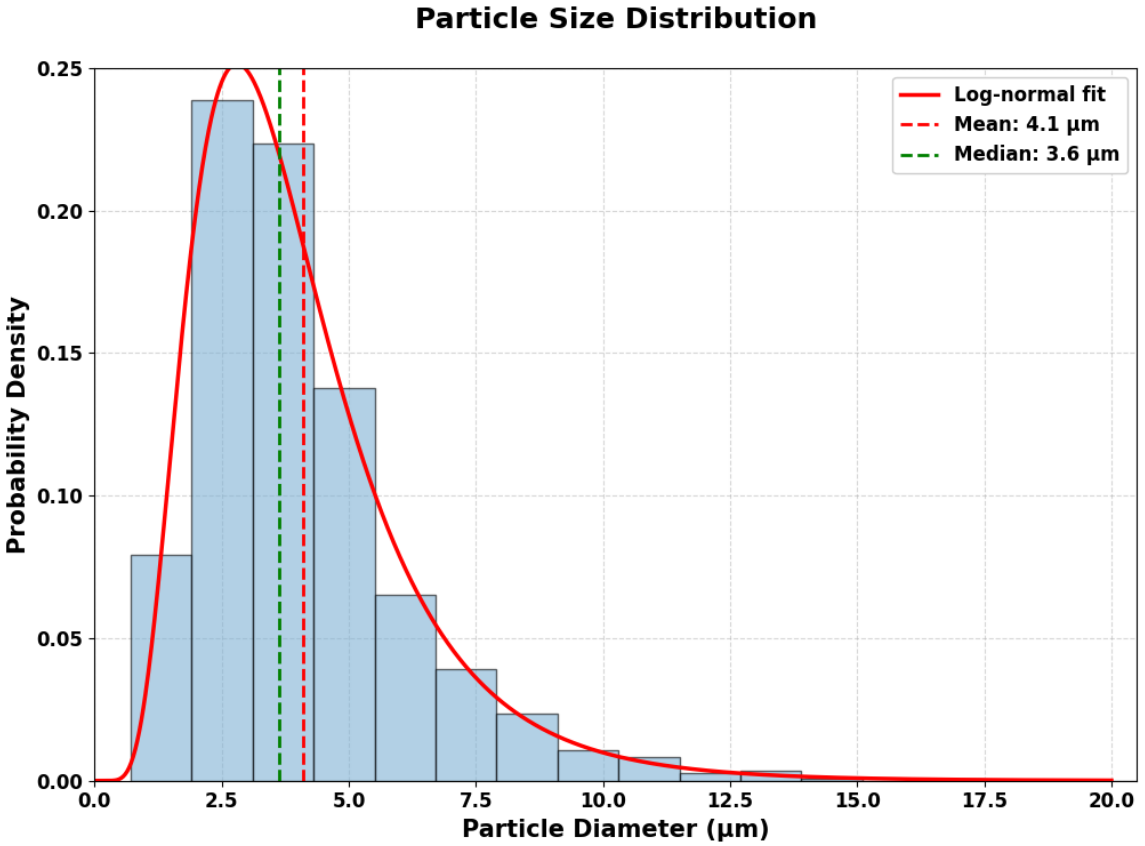


Fig. 5. Particle size distribution of avocado seed biomass

The quantitative data indicate that the particle size distribution followed a log-normal fit, with a mean of 4.2 µm and a median of 3.7 µm, revealing positive skewness (a

tail toward larger particles, since the mean exceeds the median), which is typical of grinding or precipitation processes. The probability density indicates that most particles were concentrated between 2 and 6 µm, with a moderate skew toward finer fractions. However, without values for the standard deviation, interquartile range, or cumulative percentage, it is not possible to quantify the dispersion or determine the percentage of particles outside this range.

ADSORPTION ISOTHERMS

Langmuir Model

Classical adsorption isotherms, such as the Langmuir and Freundlich isotherms, are used for aqueous adsorption studies; however, these models do not consider temperature effects (Acharya *et al*. 2026). The Langmuir isotherm is based on an assumption of individual ion adsorption onto homogeneous, non-interacting sites. The linearized plot of C_e/q_e *versus* C_e (Fig. 5) the analysis of the linearized Langmuir form (C_e/q_e *vs.* C_e) yielded an R^2 value of 0.9904, which supports the validity of the assumptions. Initial pollutant concentration, pH, temperature, and contact time, were systematically investigated to determine the optimal adsorption conditions (Aseeri *et al.* 2026).

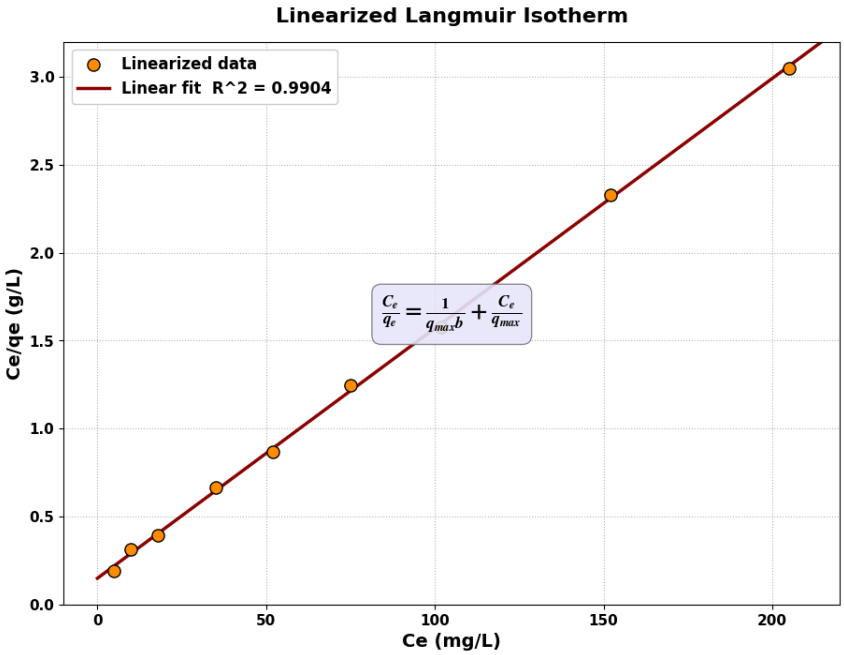


Fig. 6. Langmuir Isotherm and Linearized Langmuir Isotherm

The conventional Langmuir isotherm equation assumes an idealized homogeneous pore surface, making it insufficient to describe structure-dependent adsorption (Abu-Shareha *et al*. 2026).

Freundlich Model

The Freundlich isotherm has been known for more than a century for describing various adsorption conditions and is essential for the rational development of materials and

processes for adsorption applications, many of which are important for the transition toward sustainability (Christensen 2026).

The Freundlich isotherm, an empirical model that is interpreted as a description of multilayer adsorption on heterogeneous surfaces, was evaluated using the linear plot of logq_e *versus* logC_e (Fig. 6). The coefficient of determination, $R^2 = 0.829$, was found to be lower than that obtained with the previous model. The calculated parameters were KF = 58.7 mg/g and n = 28.6. Although the value of n > 1 indicates favorable adsorption conditions, the lower R^2 suggests that this model does not adequately fit the experimental data. Each model was simultaneously fitted to the data at the three temperatures using a two-step parameter estimation procedure combining differential evolution and optimization (Chu and Hashim 2026).

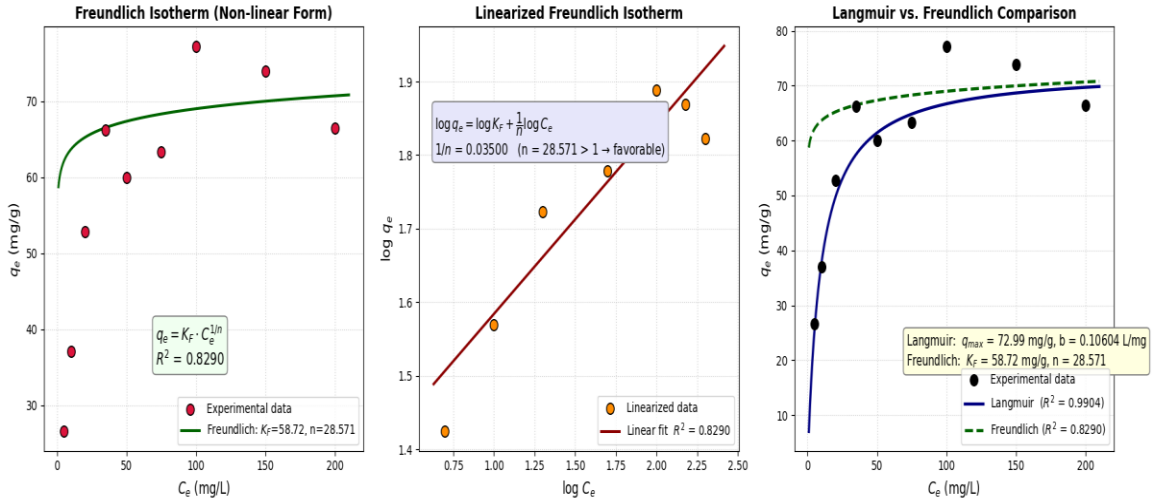


Fig. 7. Freundlich Isotherm, Linearized Freundlich Isotherm and Langmuir vs. Freundlich Comparison

Adsorption isotherms such as Langmuir and Freundlich are used for aqueous adsorption; however, these models do not consider temperature effects and operate using a mathematical equation (Abu-Shareha *et al*. 2026).

Comparison of Models

The adsorption behavior was then interpreted in terms of ideal and non-ideal adsorptions to provide a thermodynamic perspective for understanding the model parameters (Lan *et al*. 2026). When comparing both models, it is evident that the Langmuir model ($R^2 = 0.9904$) described the system more accurately than the Freundlich model ($R^2 = 0.829$). This indicates that the uptake of lead (II) by avocado seeds is consistent with monolayer adsorption onto active sites with similar energy levels. The experimental q_e values of 26.8, 58.2, 65.1, and 74.4 mg/g were closer to the Langmuir predictions of 4.4, 66.1, 70.1, and 71.1 mg/g than to the Freundlich predictions of 57.7, 68.8, 71.0, and 72.2 mg/g, reinforcing the suitability of the former. Subsequently, a mathematical model was developed using the Langmuir–Freundlich equation to predict adsorption (Abu-Shareha *et al*. 2026).

Adsorption Kinetics

Equilibrium time

The kinetic analysis was performed using an initial concentration of 494.5 mg/L, a particle size of 125 µm, a pH of 4.5, an adsorbent dose of 0.18 g, and an agitation speed of 400 rpm. A rapid increase in adsorption was observed during the first 20 min, reaching a value of 23.7 mg/g, after which it stabilized at approximately 24.0 mg/g up to 240 min. Equilibrium was reached at approximately 50 min, with no notable variations thereafter. The rapid initial phase is attributed to the abundance of available active sites on the external surface of the biosorbent.

Pseudo-first-order model

The linearized pseudo-first-order equation ($\log(q_e - q_t)$ *vs.* t) yielded an R^2 of 0.813, with $k_1 = 0.00714$ min^{-1} and a theoretical q_e of 150.6 mg/g (Fig. 7). The low coefficient of determination indicates that this model did not adequately represent the temporal evolution of the process.

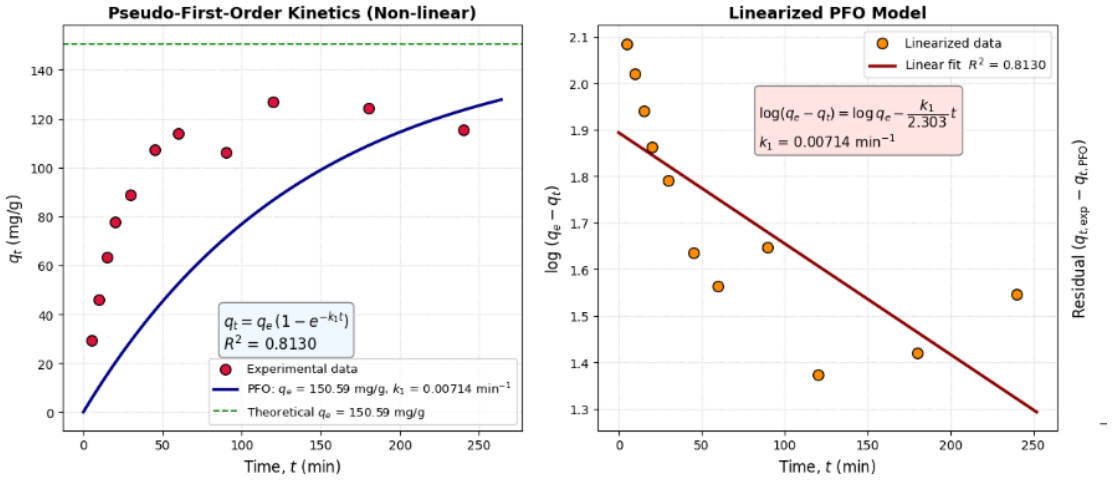


Fig. 8. Pseudo first order Kinetics and Linearized Model

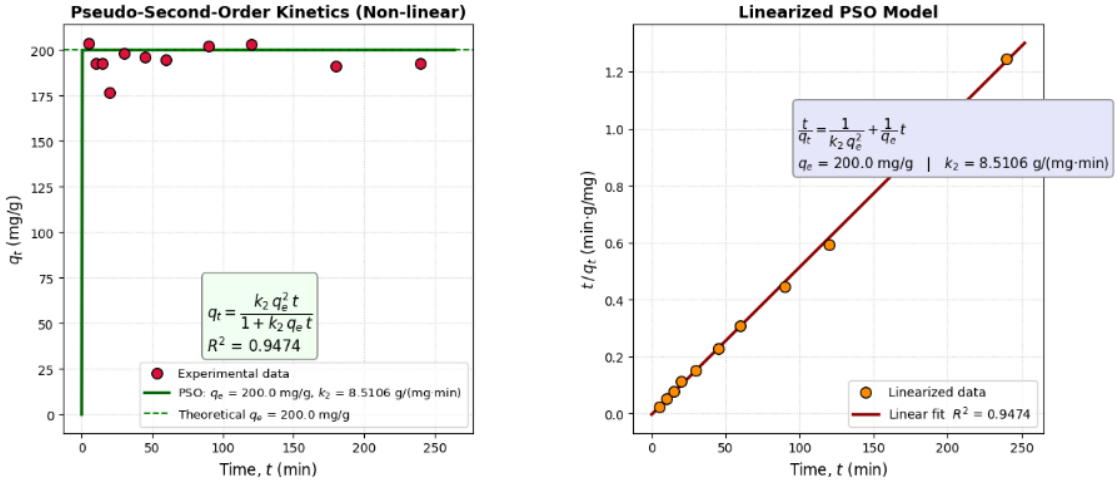


Fig. 9. Pseudo Second order Kinetics and Linearized Model

Pseudo-second-order model

In contrast, the pseudo-second-order model (t/q_t *vs*. t) showed an R^2 of 0.9474, considerably higher than that of the previous model (Fig. 8). The obtained parameters were k_2 = 8.5 g/(mg·min) and q_e = 200 mg/g.

Elovich and intraparticle diffusion models

The Elovich and intraparticle diffusion models yielded R^2 coefficients of 0.9565 and 0.9585, respectively. This can be attributed to the fact that lead(II) adsorption involves migration of the adsorbate into internal pores.

The presence of heavy metals in water bodies has become a major environmental concern, particularly when considering conventional water-quality parameters, heavy metal contamination, and sediment pollution (Islam 2026). Water contamination can become even more severe when surface and groundwater sources require increasingly intensive treatment before use (Paramanik 2026). Lead (Pb) is a neurotoxic metal that can leach into drinking water, highlighting the need to develop and implement strategies aimed at reducing its presence (Roy *et al*. 2025).

Table 1 compares the present results with those of two other recent studies. As shown, the results were in a similar range.

Table 1. Comparison of the Determined Maximum Adsorption Capacity with Recent Studies

Study	Biomass	Particle Size	Maximum Adsorption Capacity for Pb(II)
The present study (2026)	Avocado seed (*Persea americana*)	125 to 425 µm	72.9 mg/g
Cardoso *et al.* (2025)	Coconut shell (*Cocos nucifera*)	105 to 297 µm	79.2 mg/g
Ungureanu *et al.* (2024)	Apple residue after extraction	Not confirmed	48.6 mg/g

CONCLUSIONS

1. The powder of avocado seed (*Persea americana*) proved to be an effective and low-cost biosorbent for the removal of lead (II), reaching a maximum adsorption capacity of 74.4 mg/g at a particle size of 125 µm, pH 4.5, and an initial concentration of 494.5 mg/L.
2. The functional groups identified by Fourier transform infrared (FTIR) measurements could participate in the binding of metal ions, which is strictly consistent with the findings of the present study.
3. The adsorption process fitted the Langmuir model (R^2 = 0.9904) and the pseudo-second-order kinetic model (R^2 = 0.9474). It is concluded that this biosorbent represents a sustainable alternative for the treatment of lead-contaminated water.

ACKNOWLEDGEMENTS

Conflict of Interest

The authors acknowledge the Universidad Nacional Autónoma de Huanta. This research was conducted with FOCAM funding; however, there is no academic conflict of interest associated with the development of this research, and all authors and co-authors have authorized the publication of the scientific article.

REFERENCES CITED

Abu-Shareha, A. A., Alfilh, R., Yaseen, A. M., Sudhamsu, G., Sahu, P. K., Jenifer D, R., Sharma, S., Jain, V., and Hekmatyar, Z. (2026). "Robust data-driven modeling of Cd(II) adsorption on biochar," *Journal of Hazardous Materials Advances* 21, article 101004. https://doi.org/10.1016/j.hazadv.2026.101004

Acharya, A., Jeppu, G., Pai, A. D., and Acharya, S. (2026). "A temperature-modified Langmuir–Freundlich model for the adsorption of aqueous contaminants," *Journal of Water Process Engineering* 89, article 110244. https://doi.org/10.1016/j.jwpe.2026.110244

An, Z., Nzediegwu, C., Naeth, M. A., and Chang, S. X. (2026). "Monovalent-divalent element quotient influences lead(II) removal by nitric acid-modified biochars in aqueous solutions," *Results in Engineering* 32, article 112696. https://doi.org/10.1016/j.rineng.2026.112696

Anbesa, M. A., Jara, Y. S., and Adugna, D. B. (2026). "Effective adsorbents for the removal of pesticides from contaminated water," *Desalination and Water Treatment* 326, article 101813. https://doi.org/10.1016/j.dwt.2026.101813

Aseeri, A. A., Sead, F. F., Altalbawy, F. M. A., Yousif, N., Norberdiyeva, M., Sahib, A. S., Abdulali, Z. S., Alwan, M., Jawad, M., Mushtaq, H., and Al Hesani, M. (2026). "Synthesis and evaluation of a Ni-H_2bpda/Fe_3O_4 nanocomposite with high tetracycline adsorption capacity and broad-spectrum antibacterial activity," *Results in Chemistry* 25, article 103249. https://doi.org/10.1016/j.rechem.2026.103249

Cardoso, A. P., Carvalho, N. da S., Veneu, D. M., Valdiviezo-Gonzales, L., Pino, A. H., and Torem, M. L. (2025). "Comparative evaluation of lead and manganese removal from contaminated water using *Cocos nucifera* shell powder in batch and continuous adsorption systems," *South African Journal of Chemical Engineering* 53, 483-494. https://doi.org/10.1016/j.sajce.2025.06.003

Christensen, J. M. (2026). "The theoretical basis for the Freundlich adsorption isotherm," *Surface Science* 774, article 123025. https://doi.org/10.1016/j.susc.2026.123025

Chu, K. H., and Hashim, M. A. (2026). "Modeling the temperature dependence of PFAS adsorption equilibria on activated carbon," *Next Chemical Engineering* 3, article 100106. https://doi.org/10.1016/j.nxcen.2026.100106

Dong, X., Wang, Y., Zhang, S., Shi, C., and Hu, F. (2026). "pH-switchable magnetic biomass-derived adsorbent for selective removal of oppositely charged dyes," *Industrial Crops and Products* 249, article 123752. https://doi.org/10.1016/j.indcrop.2026.123752

Giraldo, J. F. R., and Marin, J. E. G. (2025). "Application of Fourier transform infrared spectroscopy (FTIR) for protozoan analysis: A systematic review," *Photodiagnosis*

and Photodynamic Therapy 51, article 104441. https://doi.org/10.1016/j.pdpdt.2024.104441

He, W.-M., Hao, G.-S., Wang, S.-Q., Meng, R., Wang, D., Wang, Y., and Xu, B.-J. (2026). "Machine learning-enhanced attenuated total reflectance Fourier transform infrared (ATR-FTIR) spectroscopy for discrimination of green Arabica and Robusta coffee beans," *Journal of Agriculture and Food Research* 26, article 102689. https://doi.org/10.1016/j.jafr.2026.102689

Hira, N. e, Lock, S. S. M., Lim, L. G., Arshad, U., Darban, M. A., Farooqi, A. S., Ilyas, S. U., and Yiin, C. L. (2025). "Molecular simulation and ANN modelling for cadmium (Cd) and lead (Pb) adsorption from water using zeolites," *Results in Engineering* 25, article 104517. https://doi.org/10.1016/j.rineng.2025.104517

Huang, J.-L., Li, Z.-Y., Mao, J.-Y., Chen, Z.-M., Liu, H.-L., Liang, G.-Y., Zhang, D.-B., Wen, P.-J., Mo, Z.-Y., and Jiang, Y.-M. (2024). "Contamination and health risks brought by arsenic, lead and cadmium in a water-soil-plant system nearby a non-ferrous metal mining area," *Ecotoxicology and Environmental Safety* 270, article 115873. https://doi.org/10.1016/j.ecoenv.2023.115873

Islam, F. A. S. (2026). "Integrated pollution regimes and water resource sustainability across Bangladeshi rivers and aquifers," *Cleaner Water* 8, article 100309. https://doi.org/10.1016/j.clwat.2026.100309

Jjagwe, J., Olupot, P. W., Kulabako, R., and Carrara, S. (2026). "Magnetite-activated carbon nanocomposite derived from steel waste and rice husks for trace removal of Pb(II) and Cd(II) from drinking water: Synthesis, characterization, and adsorption performance," *Chemical Engineering Journal: Green and Sustainable* 3, article 100116. https://doi.org/10.1016/j.cejgas.2026.100116

Lan, W., Li, S., and Deng, S. (2026). "Cluster adsorption Langmuir model (CALM) for CO2 adsorption of carbon capture: From ideal to real adsorption," *Carbon Capture Science and Technology* 19, article 100630. https://doi.org/10.1016/j.ccst.2026.100630

Li, H., Sun, Y., Liu, Y., Liu, Q., Duan, Y., Zhou, L., Cai, H., Yang, W., Hamilton, D. P., Paerl, H. W. *et al*. (2026). "Taste and odor in water supplies: A review of producers, adverse effects, detection, and mitigation," *Water Biology and Security* 2026, article 100608. https://doi.org/10.1016/j.watbs.2026.100608

Li, Z., Lu, G., Du, D., and Zhao, D. (2025). "Harnessing low-cost adsorbents for removal of heavy metals and metalloids in contaminated water: Progress in the past decade and future perspectives," *Journal of Cleaner Production* 518, article 145845. https://doi.org/10.1016/j.jclepro.2025.145845

Molla, A., Khatun, N., and Kim, D. (2026). "Biomass-derived carbon materials as adsorbent materials for CO2, organic dyes, antibiotics, and heavy metals—A review," *Biomass Futures* 2, article 100036. https://doi.org/10.1016/j.bmf.2026.100036

Paramanik, M. (2026). "Pollution amplifies global water scarcity and hinders progress towards Sustainable Development Goal 6," *Next Materials* 13, article 103227. https://doi.org/10.1016/j.nxmate.2026.103227

Reus, S., Krebbers, L., Radosavljević, A., van Bommel, M. R., and van den Berg, K. J. (2026). "Ageing of Prussian blue oil paints: The effect of the pigment studied using attenuated total reflection Fourier transform infrared spectroscopy," *Vibrational Spectroscopy* 143, article 103899. https://doi.org/10.1016/j.vibspec.2026.103899

Roy, S., Fisher, M. B., Minyila, S., Seidu, Z., Liang, K., and Salzberg, A. A. (2025). "Preventing lead (Pb) contamination in rural community water systems in LMICs

through analytical screening, policy and standards enforcement, and supply chain interventions," *Groundwater for Sustainable Development* 31, article 101509. https://doi.org/10.1016/j.gsd.2025.101509

Sharma, G., Verma, Y., Lai, C. W., Naushad, Mu., Iqbal, J., Kumar, A., and Dhiman, P. (2024). "Biochar and biosorbents derived from biomass for arsenic remediation," *Heliyon* 10, article e36288. https://doi.org/10.1016/j.heliyon.2024.e36288

Ungureanu, G., Enache, I.-M., Cara, I. G., Motrescu, I., and Patras, A. (2024). "Insights into the environmental benefits of using apple pomace for biosorption of lead from contaminated water," *Heliyon* 10(17), article e36811. https://doi.org/10.1016/j.heliyon.2024.e36811

Vera-Marmanillo, V., Pilares, L. A., and Vergara, R. Z. (2026). "Adsorption capacity of biochar and leonardite for lead removal Pb2+ from water," *Carbon Trends* 24, article 100682. https://doi.org/10.1016/j.cartre.2026.100682

Wang, K., Kou, Y., Wang, K., Guo, C., Liang, X., Wang, M., Wang, W., and Wang, J. (2025). "Comparative study on the adsorption and desorption behaviors of quinolone pollutants on polystyrene microplastics of different particle sizes," *Environmental Technology and Innovation* 38, article 104216. https://doi.org/10.1016/j.eti.2025.104216

Xia, J., Mao, Y., Zhou, M., Deng, S., and Shi, X. (2026). "Laboratory experiment on phosphorus adsorption characteristics of different-sized sediment particles in the Middle Yangtze River," *International Journal of Sediment Research* 41(5), article 7. https://doi.org/10.1016/j.ijsrc.2026.07.007

Zhang, Y., Ma, T., Hou, Y., and Wang, A. (2026). "Study on oxygen adsorption characteristics and structure-activity relationship mechanism of coal during the initial stage of low-temperature oxidation," *Process Safety and Environmental Protection* 208, article 108440. https://doi.org/10.1016/j.psep.2026.108440

Zhang, Z., and Shu, Y. (2025). "An optimized method for solution of fixed-bed adsorption model considering particle-size distribution via method of characteristics," *Chemical Engineering Journal Advances* 24, article 100926. https://doi.org/10.1016/j.ceja.2025.100926

Article submitted: September 15, 2026; Peer review completed: October 17, 2026; Revised version received: October 19, 2026; Accepted: October 22, 2026; Published: November 11, 2026.
DOI: 10.15376/biores.22.1.169-183